Christine Julia Lange

Surface-Enhanced Raman Spectroscopy for Environmental Monitoring

Explaining the large signal enhancements in SERS using the Drude-Lorentz model for a spherical particle with dielectric properties and selected SERS applications from the environmental sciences

Bachelor's thesis in Theoretical and Environmental Chemistry
Supervisor: Rosario Roberto Riso
April 2023
Word count: 5333

Norwegian University of Science and Technology
Faculty of Natural Sciences
Department of Chemistry

NTNU

Contents

1 Summary

In this thesis, the principles of surface-enhanced Raman spectroscopy (SERS) are explored with a focus on the role of dielectric response in modifying the local electric field around a nanosphere. The Drude-Lorentz model is utilized to derive an expression for the complex dielectric function, specifically for gold and silver as these are the two most common SERS substrate materials. Some technical challenges of the technique are discussed, especially fluorescent interference which can mask the Raman signal. Finally, three contemporary examples of SERS applications in environmental monitoring are presented to demonstrate some of its practical use and potential for the future.

2 Introduction

Surface-enhanced Raman spectroscopy (SERS) is a powerful analytical technique used to perform Raman measurements for very small molecular concentrations. The Raman effect, discovered and described by Chandrasekhara Raman in 1928, is the inelastic scattering of photons from a surface. Electrons in a molecule hit by (laser) photons are excited to a higher energy level, and at the same time, chemical bonds receive vibrational energy. As a result, the scattered (re-emitted) photons (called the Raman photons) are shifted in frequency. By measuring the energy of the scattered photons, information about the vibrational modes of the molecule can be obtained, which then can be used to identify it. When the energy transfer is from the photon to the molecule, the frequency of the Raman photons is lower than the incident radiation (**Stokes scattering**). When the molecule transfers energy to the photon, the frequency is higher (**Anti-Stokes scattering**). Thus, the Raman shift can have both signs [18].

Raman spectroscopy has many advantages over other spectroscopy methods, for example that it is non-destructive, requires minimal sample preparation and that it can be used to analyze samples in situ. However, the Raman effect is very weak; typically, only one out of 10^6 photons undergoes inelastic scattering. SERS aims to amplify the Raman signals by several orders of magnitude. This can be achieved by letting the molecular species to be detected (the probe, the target molecule(s)) adsorb on, or at least be in close proximity to, a **SERS substrate**. This substrate is made of metallic nanostructures that can interact with an electromagnetic field. The interaction can produce large amplifications of the field through excitations known as **plasmon resonances** [18]. The principles of SERS are illustrated for some nanoplastics target molecules in figure 1 [29]. In addition to the problem that the Raman effect is weak, there is of course also the problem that elastic **Rayleigh scattering** is occurring all the time. Rayleigh scattering is a problem in SERS because it causes background signals that can overwhelm the Raman signals with respect to intensity. Careful filtering of the Rayleigh photons (at Raman shift zero) is thus required [21].

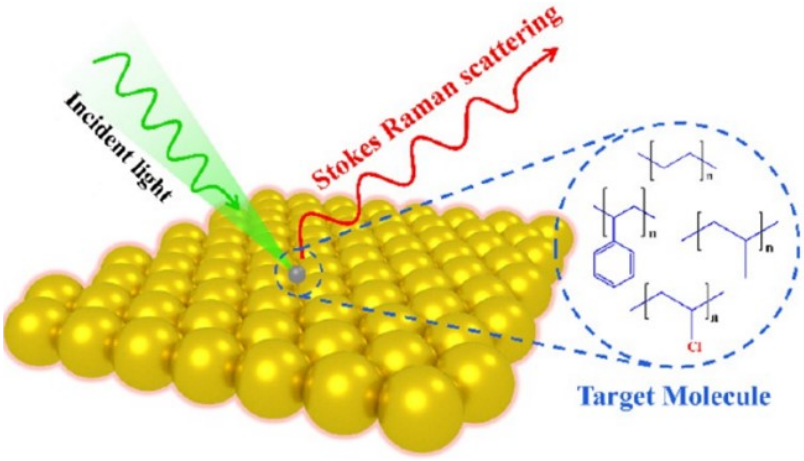

Figure 1: Schematic illustration of the principles of SERS. The inelastic scattering of light is greatly enhanced by metallic nanoparticles (illustrated as golden spheres). Figure taken from article [29].

Signals from standard Raman spectroscopy are only detectable for concentrations above the macromolar range and for particles bigger than about 1 µm in size [26]. For some applications, e.g. the

detection of nanoplastics, better resolutions are needed because the particles may be smaller than the detection limit or the concentrations are very low. Research suggests that even small concentrations of nanoplastics can have adverse effects on human health [1]. SERS allows us to improve the spectral resolution to the limit of single molecule sensing [16]. The theoretical description of the nanoparticles making up the SERS substrate usually relies on the concept of dielectric materials. In principle, dielectrics do not conduct electricity, but are polarized when subject to an external electric field. These media modify and enhance the electric field close to their surface and these enhanced fields play a critical role in the SERS phenomenon.

The **dielectric constant** is a measure of the ability of a material to store electrical energy in an electric field. It reflects the degree of polarization of the material when subjected to an electric field and is defined as the electric flux density in a material to the electric flux density in vacuum. This constant is the zero frequency case of the **dielectric function**, which is a dynamic property that describes how a material responds to an electromagnetic field at different frequencies [1, 7].

In this thesis, the theory of **electrostatics** will be employed to analyze the response of a linear nanosphere of dielectric material to an applied electric field. The role of the dielectric response in modifying the local electric field around the metallic nanostructure in SERS will be explored as an attempt to explain the large enhancement factor. Furthermore, the Drude-Lorentz model will be explained and utilized to derive an expression for the complex dielectric function of relevant materials/elements in SERS substrates. Some of the technique's drawbacks and technical challenges will be discussed, particularly the effect of fluorescent interference. Finally, three examples of contemporary research on potential applications of SERS in environmental monitoring will briefly be discussed. These examples are presented to concretely illustrate how SERS is practically used today as well as to reflect around how it could play an increasingly important role in environmental monitoring in the future.

3 Theory

Unless stated otherwise, most of the electrostatics theory (parts 3.1-3.5) is taken from Griffiths' *Introduction to Electrodynamics* [7].

3.1 Dielectrics and Polarization

Most solids can by good approximation be divided into two large classes of matter: conductors and insulators. **Dielectrics** are an important subcategory of insulators that are polarizable. In conductors, electrons are said to roam around more or less freely within a material. In dielectrics, on the other hand, electrons are attached to specific atoms or molecules and can only move a little bit within these. These microscopic displacements of electrons are not as dramatic as charge rearrangements in conductors, but their cumulative effects account for the characteristic behaviours of dielectric materials.

When a piece of dielectric material is placed in an electric field, small dipole moments will be induced in each of the material's molecules. These microscopic dipoles all line up and point in the direction of the field, resulting in a polarized material. The dipole moment per unit volume, $\mathbf{P}$, is called the **polarization**. It can be written as:

$$\mathbf{P} = \frac{1}{\text{Vol}} \sum_i q_i \mathbf{x}_i, \tag{1}$$

where q_i is the charge of the ith particle, $\mathbf{x}_i$ is its position vector, and Vol is the volume of the material.

3.2 The Electric Field and Potential

Electric fields are created and "felt" by charged objects. The force between charges is described by Coulomb's law. The magnitude of the electric and field of a point charge decreases with a factor proportional to the inverse of the distance squared [22]. An electric field $\mathbf{E}$ is a vector function whose curl is zero in the absence of time-varying magnetic fields (i.e. $\nabla \times \mathbf{E} = 0$). It follows from Stokes' theorem that the line integral of $\mathbf{E}$ around any closed loop is zero. A consequence of this is that the electric field can be written as the gradient of some scalar function V:

$$\mathbf{E} = -\nabla V, \tag{2}$$

where V is the electric potential. As will be demonstrated later, this relationship is particularly useful when computing the electric field. Another very useful and fundamental equation regarding electric fields is **Gauss' law**. In differential form, it states:

$$\nabla \cdot \mathbf{E} = \frac{1}{\epsilon_0} \rho, \tag{3}$$

where ϵ_0 is the **vacuum permittivity**, equal to about $8.854 \cdot 10^{-12}$ C^2 $\text{N}^{-1}\text{m}^{-2}$, and ρ is the charge density. In simple terms, this equation relates the distribution of electric charge to the behavior of the electric field around that distribution. Inserting equation (2) into Gauss' law gives

$$\nabla^2 V = -\frac{\rho}{\epsilon_0}, \tag{4}$$

which is known as **Poisson's equation**. In regions where there is no charge, i.e. where $\rho = 0$, this equation becomes simply $\nabla^2 V = 0$. This is known as the **Laplace equation** and it is discussed below.

3.3 The Laplace Equation and its Solutions

Laplace's equation is a second-order partial differential equation describing the behaviour of V in a region of space where there are no charges. It can be written as

$$\nabla^2 V = \frac{\partial^2 V}{\partial x^2} + \frac{\partial^2 V}{\partial y^2} + \frac{\partial^2 V}{\partial z^2} = 0, \tag{5}$$

in a three-dimensional Cartesian coordinate system. For round potentials (spheres), it is more convenient to use spherical coordinates, such that the Laplace equation becomes:

$$\frac{1}{r^2}\frac{\partial}{\partial r}(r^2\frac{\partial V}{\partial r}) + \frac{1}{r^2\sin\theta}\frac{\partial}{\partial \theta}(\sin\theta\frac{\partial V}{\partial \theta}) + \frac{1}{r^2\sin^2\theta}\frac{\partial^2 V}{\partial \phi^2} = 0. \tag{6}$$

An illustration of spherical coordinates is given in Figure 2. Assuming an **azimuthal symmetry**, i.e. that V is independent of ϕ, simplifies equation (6) to the first two terms. Separation of variables converts this partial differential equation into an ordinary differential equation. The solutions are written as products of two terms:

$$V(r,\theta) = R(r)\ \Theta(\theta). \tag{7}$$

The first term, known as the **radial part** of the solution, depends only on r. The general solution for the radial part is:

$$R(r) = Ar^l + \frac{B}{r^{l+1}}, \tag{8}$$

where A and B are constants and l is a positive integer that refers to the angular momentum. The solution to the **angular part** $\Theta(\theta)$ is given by the so-called Legendre polynomials $P_l(x)$ of variable $\cos(\theta)$. These polynomials are orthogonal polynomials and can be defined by the Rodrigues formula:

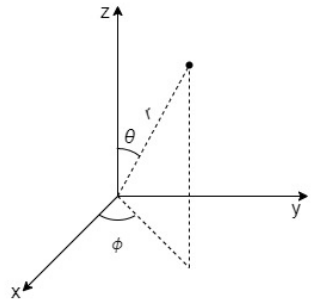

Figure 2: Spherical coordinates, with $(x, y, z) = (r, \theta, \phi)$ Figure drawn in draw.io

$$P_l(x) = \frac{1}{2^l l!}(\frac{d}{dx})^l(x^2-1)^l. \tag{9}$$

The general solution to the Laplace equation (7) can thus be written as:

$$V(r,\theta) = \sum_{l=0}^{\infty}\left(A_l r^l + \frac{B_l}{r^{l+1}}\right)P_l(\cos\theta). \tag{10}$$

This is the so-called **multipole expansion** of the potential. The coefficients A_l and B_l depend on the details of the charge distribution. These are determined by solving the boundary value problem that arises by applying the Laplace equation to the region of interest. These can be equal to zero if the potential satisfies certain symmetry conditions as discussed below. The coefficient l is called the "multipole moment" of the electric potential. The monopole moment ($l = 0$) corresponds to a point charge, the **dipole moment ($l = 1$)** corresponds to a pair of opposite charges separated by a distance, the quadrupole moment ($l = 2$) corresponds to a distribution of charges with a quadrupolar symmetry, and so on.

3.4 Linear Dielectrics and Permittivity

If the total electric field is not too strong, the polarization is proportional to the electric field for many materials:

$$\mathbf{P} = \epsilon_0 \chi_e \mathbf{E}. \tag{11}$$

The dimensionless constant of proportionality, χ_e, is called the **electric susceptibility** of the medium. Its value depends on the electric properties (the microscopic structure) of the material. Materials obeying equation (11) are called **linear dielectrics**. Examples of linear dielectric materials include glass, rubber, and plastic.

A **free charge** is a charge that is not a result of polarization, while a **bound charge** is a polarization charge, induced by the presence of an electromagnetic (EM) field. The **electric displacement D** is a measure of the electric flux that passes through a given area. It is directly related to the charge density of the material and takes both free and bound charges under consideration. **D** is related to the electric field as follows:

$$\mathbf{D} = \epsilon_0 \mathbf{E} + \mathbf{P}. \tag{12}$$

Inserting equation (11) into (12):

$$\mathbf{D} = \epsilon_0 \mathbf{E} + \epsilon_0 \chi_e \mathbf{E} \tag{13}$$

$$= \epsilon_0 (1 + \chi_e)\mathbf{E} = \epsilon_0 \epsilon_r \mathbf{E} = \epsilon \mathbf{E}, \tag{14}$$

connects **D** to the so-called **permittivity** ϵ and **dielectric constant** (relative permittivity) ϵ_r. Permittivity is a measure of a material's ability to store electric charge in an electric field, while the dielectric constant indicates how much the electric field inside a material is reduced compared to the electric field in vacuum. The medium outside the sphere in the computations below is treated as a vacuum.

3.5 The Electric Field inside a Polarized Nanosphere

A nanosphere of some linear, homogeneous dielectric material is placed in a uniform electric field **E** in the z-direction (see Figure 3). The resulting electric field inside and around the sphere can be found by solving the Laplace equation with appropriate boundary conditions.

If R is the (fixed) radius of the sphere, and r is the radial distance from its center to some arbitrary point, then two different potentials $V_{\text{in}}(r, \theta)$ for $r \leq R$ and $V_{\text{out}}(r, \theta)$ for $r \geq R$ can be defined. Here, V_{in} and V_{out} are the potentials inside and outside (i.e. around) the sphere, respectively. The boundary in this case is defined to be the surface of the sphere, and the boundary conditions are:

$$\left.\begin{array}{lll} (i) & V_{\text{in}} = V_{\text{out}} & \text{for } r = R, \\ (ii) & \epsilon_r \dfrac{\partial V_{\text{in}}}{\partial r} = \dfrac{\partial V_{\text{out}}}{\partial r} & \text{for } r = R, \\ (iii) & V_{\text{out}} \to -Er\cos\theta & \text{for } r \gg R. \end{array}\right\} \tag{15}$$

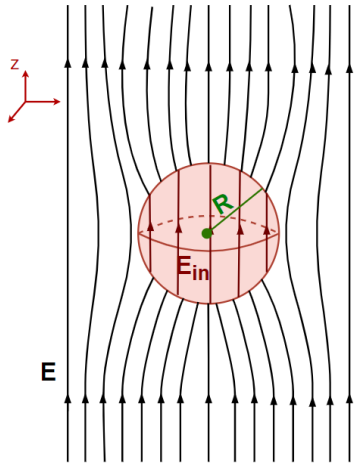

Figure 3: Graphical illustration: A sphere in a uniform electric field **E**. The induced field inside the sphere is $\mathbf{E}_{\text{in}}$. Figure drawn in *draw.io*

The second boundary condition arises from Stokes' theorem under the assumption that there is no free charge at the surface of the sphere. Using equation (10), the potential inside the sphere is given as:

$$V_{\text{in}}(r,\theta) = \sum_{l=0}^{\infty} A_l r^l P_l(\cos\theta) \qquad \text{for } 0 \le r < R. \tag{16}$$

All B_l coefficients must be equal to zero because otherwise the electric potential would diverge when r approaches zero. This cannot be the case as there are no free charges inside the dielectric sphere and the Laplace equation (eq. (5)) has only finite solutions. Outside the sphere the potential is:

$$V_{\text{out}}(r,\theta) = -Er\cos\theta + \sum_{l=0}^{\infty} \frac{B_l}{r^{l+1}} P_l(\cos\theta) \qquad \text{for } R < r < \infty. \tag{17}$$

Here, all A_l coefficients except for $l = 1$ must be zero, because for large r, the electric field approaches a constant field in the z-direction. Thus, $A_1 = -E$, leaving only $-Er\cos(\theta) = -Ez$ for the A_l-term. At $r = R$, $V_{\text{in}} = V_{\text{out}}$, so by equating (16) and (17) we get:

$$\left.\begin{aligned} A_l R^l &= \frac{B_l}{R^{l+1}} && \text{for } l \neq 1, \\ A_1 R &= -ER + \frac{B_1}{R^2} && \text{for } l = 1. \end{aligned}\right\} \tag{18}$$

By comparing coefficients in the sums of V_{in} and V_{out} above, boundary condition (ii) gives

$$\left.\begin{aligned} A_l &= B_l = 0 && \text{for } l \neq 1, \\ A_1 &= -\frac{3}{\epsilon_r + 2} E \text{ and } B_1 = \frac{\epsilon_r - 1}{\epsilon_r + 2} R^3 E && \text{for } l = 1. \end{aligned}\right\} \tag{19}$$

Thus, we need only consider $l = 1$, i.e. the dipole moment. The dipole moment is responsible for the polarization and thereby modification of the electric field inside and outside the dielectric sphere. For $l = 1$, the Legendre polynomial is $P_1(x) = x$, so $P_1(\cos\theta) = \cos\theta$. Equation (16) can thus be simplified to

$$V_{in}(r,\theta) = -\frac{3E}{\epsilon_r + 2} r\cos\theta = -\frac{3E}{\epsilon_r + 2} z. \tag{20}$$

Since the electric field can be found by taking the gradient of the potential (equation (2)), the electric field inside the sphere is

$$\mathbf{E}_{\text{in}} = \frac{3}{\epsilon_r + 2}\mathbf{E} \tag{21}$$

in the z-direction. Similarly, we can find the field outside of the sphere by first calculating the potential:

$$V_{\text{out}}(r,\theta) = \frac{B_1}{r^2}\cos\theta - Er\cos\theta = Ez\left(\frac{\epsilon_r - 1}{\epsilon_r + 2}\frac{R^3}{r^3} - 1\right). \tag{22}$$

Taking the gradient of this expression is a bit less straightforward than it was for V_{in}, but the analytical solution is:

$$\mathbf{E}_{\text{out}}(\mathbf{r}) = \left(\hat{\mathbf{z}} - \left(\frac{\epsilon_r - 1}{\epsilon_r + 2}\right) R^3 \left[\frac{\hat{\mathbf{z}}}{r^3} - \frac{3z}{r^5}\mathbf{r}\right]\right) E, \tag{23}$$

where $\mathbf{r}$ is the position vector. The position can also be written with the Cartesian unit vectors $\hat{\mathbf{x}}$, $\hat{\mathbf{y}}$ and $\hat{\mathbf{z}}$; $\mathbf{r} = x\hat{\mathbf{x}} + y\hat{\mathbf{y}} + z\hat{\mathbf{z}}$ [25]. Now that we have a solution for the field outside the spherical nanoparticle, ϵ_r can be modeled using the Drude-Lorentz model described in the next section.

3.6 The Drude-Lorentz Oscillator Model

The Drude-Lorentz (DL) oscillator model [6] provides a useful framework for understanding the dielectric response of materials, including dielectric spheres. In the model, an electron is connected to the nucleus via an imaginary spring with some spring constant k. The material is considered to be a collection of many microscopic (Lorentz) oscillators, which can be modeled as a set of *damped harmonic* oscillators. When the sphere is placed in an electromagnetic field, the absorbed energy results in the "oscillators" oscillating at their resonant frequency. The polarization of the sphere (which is induced by the electric field) is proportional to the field and can be expressed as a sum of the contributions from the oscillators. It is this polarization which gives rise to the modified electric field within the sphere (see Figure (3)). The polarization $\mathbf{P}$ of a linear dielectric is given by equation (11), while the more general definition of $\mathbf{P}$ is given by equation (1). Inserting the general definition of polarization into equation (13) gives:

$$\mathbf{D} = \epsilon_0 \epsilon_r \mathbf{E} = \epsilon_0 \mathbf{E} + \frac{1}{\text{Vol}} \sum_i q_i \mathbf{x}_i(t) \tag{24}$$

$$\epsilon_r \mathbf{E} = \mathbf{E} + \frac{1}{\text{Vol}} \sum_i \frac{e \cdot \mathbf{x}_i(t)}{\epsilon_0} \tag{25}$$

$$\epsilon_r = 1 + \frac{1}{\text{Vol}} \sum_i \frac{e \cdot x_i^z(t)}{\epsilon_0 |\mathbf{E}|}. \tag{26}$$

Here, we assume that $\mathbf{E}$ and $x_i^z(t)$ point in the z-direction. The charge q_i was replaced by e, the elementary charge, since we are only looking at electrons. The remaining task now is to find a solution to the position $x_i(t)$. This is done by solving the differential equation of a damped and driven harmonic oscillator problem. Figure (4) illustrates the forces acting on an electron with mass m_e. The external force arises from the applied electric field, the friction force is due to the **damping** γ and the spring force arises from the interactions between the nucleus and electron. By Newton's law, these force are equal to $m_e \ddot{x}$, thereby yielding the following differential equation:

$$\frac{d^2x}{dt^2} + \frac{\gamma}{m_e}\frac{dx}{dt} + \frac{k}{m_e}x = \frac{-e\mathbf{E}}{m_e}. \tag{27}$$

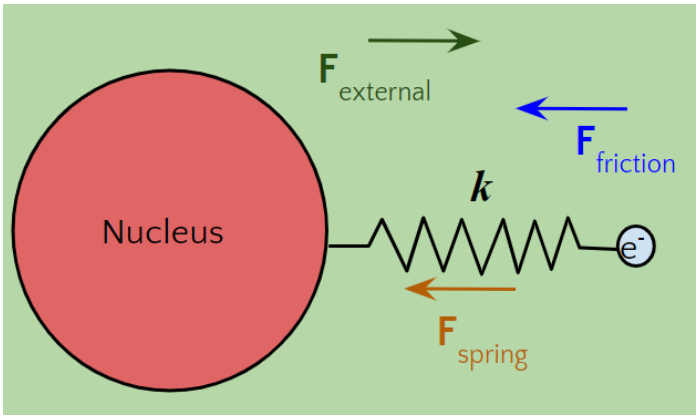

Figure 4: Simple two-dimensional illustration of the DL oscillator model. $\mathbf{F}_{external} = q_e\mathbf{E}$, $\mathbf{F}_{friction} = -\gamma\dot{x}$, $\mathbf{F}_{spring} = -kx$ when defining the x-axis from left to right. Rearranging these forces and setting them equal to $m_e\ddot{x}$ gives equation (27). Figure drawn in *Google Drawings*.

We assume the electric field $\mathbf{E}$ can be modelled as:

$$\mathbf{E} = \mathbf{E}_0 \cdot e^{i\omega t}, \tag{28}$$

where $\mathbf{E}_0$ is the field vector, assumed to point in the positive z-direction with constant amplitude, ω is the **angular frequency** of the wave and i is the imaginary unit. The representation of the electric field with real and imaginary parts leads to a convenient way to show the **phase shift** arising due to the damping. In equation (28), the amplitude is not spatially dependent, i.e. the electron "feels" the same electric field at each position (quasi-static approximation). This is justified whenever $R << \lambda = \frac{c}{\omega/(2\pi)}$, where λ is the wavelength of the incident electric field. With this notation, the complete solution to equation (27) is:

$$\mathbf{z}(t) = e^{\left(-\frac{\gamma}{2m_e}t\right)}\left(A \cdot e^{\left(t\sqrt{\frac{\gamma^2-4km_e}{4m_e^2}}\right)} + B \cdot e^{\left(-t\sqrt{\frac{\gamma^2-4km_e}{4m_e^2}}\right)}\right) + \frac{e\mathbf{E}_0 e^{i\omega t}}{k - m_e\omega^2 + i\gamma\omega}, \tag{29}$$

where A and B are constants determined by the initial conditions [20]. However, we assume *under*-damping, i.e.

$$\gamma^2 - 4km_e < 0. \tag{30}$$

This means the first part of equation (29) is oscillatory with decaying amplitude. For large t, only the particular solution $\mathbf{z}_p(t)$ remains:

$$\mathbf{z}_p(t) = \frac{e\mathbf{E}_0 e^{i\omega t}}{m_e}\frac{1}{\omega_0^2 - \omega^2 + i\omega\gamma/m_e}. \tag{31}$$

Here, the spring constant is expressed in terms of its **resonant frequency**, $\omega_0 = \sqrt{\frac{k}{m_e}}$. The particular solution can now be used to compute the displacement of the i-th electron in the z-direction, i.e. $x_i^z(t) = \mathbf{z}_p(t)$. Substituting the particular solution into the expression for relative permittivity (equation (26)) yields the following:

$$\epsilon_r = 1 + \frac{1}{\text{Vol}}\sum_i \frac{e \cdot \mathbf{z}_p(t)}{\epsilon_0|\mathbf{E}|} = 1 + (\frac{Ne^2}{m_e\epsilon_0})\frac{1}{\omega_0^2 - \omega^2 + i\omega\gamma/m_e}, \tag{32}$$

where N is the number of induced dipoles per volume. Next, we define the **plasma frequency**, ω_p;

$$\omega_p = \sqrt{\frac{Ne^2}{m_e\epsilon_0}} \tag{33}$$

yielding

$$\epsilon_r(\omega) = 1 + \frac{\omega_p^2}{\omega_0^2 - \omega^2 + i\omega\gamma/m_e}, \tag{34}$$

which shows how the dielectric constant of the sphere (or any material) is dependent on the frequency of the field it is subjected to. It is commonly called the **dielectric function** [4]. It is convenient to separate real and imaginary parts of the function:

$$\epsilon_r(\omega) = \text{Re}(\epsilon_r(\omega)) + i\text{Im}(\epsilon_r(\omega)), \tag{35}$$

where

$$\mathrm{Re}(\epsilon_r(\omega)) = 1 + \frac{\omega_p^2}{\omega_0^2 - \omega^2 + \frac{\omega^2\gamma^2}{m_e^2(\omega_0^2-\omega^2)}} \tag{36}$$

and

$$\mathrm{Im}(\epsilon_r(\omega)) = -\frac{\omega_p^2\omega\gamma}{m_e(\omega_0^2 - \omega^2)^2 + \frac{\omega^2\gamma^2}{m_e}}. \tag{37}$$

The two parts behave quite differently as a function of ω: for typical frequencies, the real part can change sign and reach large absolute values (resonance denominator), in particular if the damping parameter γ is small, whereas the imaginary part never changes sign and is usually only slowly varying for optical frequencies. The real part of ϵ_r represents the polarization response of the material while the imaginary part represents the absorption.

3.7 The Signal Enhancement in SERS

3.7.1 SERS Mechanism and Enhancement Factor

As mentioned before, SERS can enhance the Raman signal of molecules by several orders of magnitude. The mechanism behind this enhancement is complex and up to this day not well-understood, i.e. numerical simulations do not reliably coincide with experimental results [9]. The proposed mechanisms are often split into two parts; an electromagnetic (EM) enhancement and a chemical enhancement. The latter is due to the electron transfers between the analyte molecule and the nanostructure surface. Various experiments show that this enhancement mechanism is strongest for molecules adsorbed in the first layer of the substrate (**first-layer effect**) [25]. The EM enhancement mechanism is generated by localised surface plasmon resonance (**LSPR**) in the vicinity of the surface [27]. A **plasmon** is a quasiparticle consisting of collective oscillations of electrons, driven by the EM field. In dielectric materials, it is the collective oscillations of *bound* electrons within the atoms that generate the plasmons. Localised surface plasmons (**LSPs**) are plasmons confined to the surface of a nanostructure. When they are in resonance with the incident radiation, we talk about LSPR. A rigorous treatment of the LSPR effect requires a quantum mechanical (atomistic) approach. The DL model is, however, a *classical* model developed before the advent of quantum mechanics. Nevertheless, it can still provide reliable results which capture the essential properties of the dielectric function and conductivity of metal elements.

The total enhancement factor, EF, in SERS can be written as:

$$|EF|^2 = \left|\frac{\mathbf{E}_{out}(\omega)}{\mathbf{E}(\omega)}\right|^2 \cdot \left|\frac{\mathbf{E}_{out}(\omega_R)}{\mathbf{E}(\omega_R)}\right|^2, \tag{38}$$

where ω_R is the Raman shift frequency [25, 31].

Both the sphere of linear dielectric material and the Drude-Lorentz model discussed above, are of course only *approximations*. They thus simplify the complex mechanisms that actually occur in SERS. These approximations are nevertheless a good starting point to explain the enhancement factor qualitatively. The electric field response can be altered by varying two main parameters, namely; the incident electric field and the SERS substrate composition. Other factors such as substrate shape, temperature, incident angle, laser power and exposure time can also alter the response, but those parameters are not explicitly considered here.

3.7.2 The Dielectric Response of the SERS Substrate to the Incident Field

A SERS substrate is the material or surface on which the sample is adsorbed/deposited in order to enhance the Raman scattering signal. The development of SERS substrates remains an active area of research. The use of *nanomaterials* (specifically nanospheres, as discussed) as substrates is apt in many ways. The high surface area-to-volume of nanomaterials provides a large number of active sites (called **hot-spots**) for the adsorption of analyte molecules. A high and dense number of active sites means that analyte molecules are more likely to be sufficiently near a hot-spot. Additionally, the small size of nanomaterials facilitates the penetration of molecules into interstitial spaces, thereby further increasing the effective surface area [16]. Equation (23) reveals how the induced electric field (E_{out}) decreases drastically when the radial distance increases. Assuming all other parameters are constant, it is the r^{-5} term that dominates for small distances. The obtained signal is proportional to the field squared ($|E_{\text{out}}|^2$), i.e. the enhancement decreases with a factor of r^{-10}. The largest enhancements are thus found in the few nanometers closest to the substrate surface [23].

The enhancement is particularly strong when both the incident field (laser) and scattered fields are in resonance with the surface plasmons. The classic SERS substrates are gold (Au), silver (Ag) and to a lesser extent copper (Cu) [23]. These fulfill the resonance condition in the visible and near infrared (NIR), which is a frequency range for many common lasers. Even though these coinage metals are usually perceived as conductors, this is not strictly true at optical frequencies. Therefore, treating Cu, Ag and Au as dielectrics is justified for SERS [30].

Equation (23) demonstrates how the dielectric constant ϵ_r influences E_{out}, and equation (34) shows how ϵ_r is dependent on ω, ω_0, ω_p and γ. By changing the properties/material of the substrate, ω_0 and γ can be altered. ω_p does not depend on the substrate material directly, but rather on the number of induced dipoles per volume. E_{out} reaches a maximum when the real part of $\epsilon_r \approx -2$ [15]. This can only be achieved at a certain wavelength (λ). The imaginary part of $\epsilon_r(\omega)$ is assumed to be small and only weakly dependent on frequency. Furthermore, we assume a small damping γ, i.e. the electrons move almost completely freely. This assumption has empirically been shown to be reasonable. In one experiment, the DL model fitted to the experimentally observed dielectric function of silver worked extremely well for $\frac{\gamma/m_e}{\omega_0} \approx \frac{1}{500}$ [5]. Thus, the effect of γ can be neglected because it is so much smaller than the resonant frequency. For silver, $\epsilon_r = -2$ at a wavelength of 367 nm (820 THz) [13]. Plots of the real and imaginary parts of the dielectric function of Au and Ag are shown in Figure 5. It can be seen that λ is about 360 nm at $\text{Re}(\epsilon_r) = -2$ for both Au and Ag. The graphs illustrate how the metals are indeed suitable SERS substrates for optical laser light. It can also be seen that $\text{Im}(\epsilon_r)$ is very small for Ag at relevant λ, while somewhat bigger and more fluctuating for Au.

3.7.3 Technical Considerations Regarding Laser Wavelength

Different wavelength regions (equivalent to different frequencies ω) offer different advantages and disadvantages with respect to the achieved Raman intensity, spatial resolution, acquisition time and cost. Using a high-frequency (low wavelength) laser entails the risk of damaging or even burning the sample. Another main challenge is the noise interference caused by **fluorescence** signals arising from the analyte molecules [10]. Fluorescence is the phenomenon in which molecules absorb photons of a specific wavelength and re-emit them at a longer wavelength (via excitation and relaxation mechanisms). Fluorescence can mask the Raman scattering signals because of spectral overlap. Higher wavelengths result in lower fluorescent activity because the energy of a photon is inversely proportional to its wavelength. Therefore, using a higher wavelength than the computed

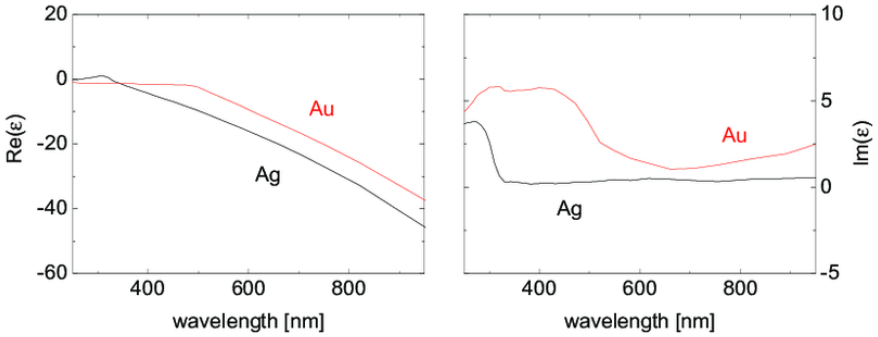

Figure 5: Dielectric function of silver and gold. The horizontal axis is the incident laser excitation wavelength λ in nm. At $\mathrm{Re}(\epsilon_r) = -2$, $\lambda \approx 360$ nm for both metals. Graph taken from article [8]

optimal wavelength obtained from the preceding theoretical model (figure 5) can be beneficial or even necessary. A trade-off between Raman intensity and fluorescence suppression must be made.

The most commonly used excitation laser is 785 nm [10, 29]. The fluorescence effect is apparent in the two Raman spectra of nicotine shown in figure 6. Even though the longer wavelength laser (785 nm) results in a lower Raman intensity (lower EF), it reveals a more detailed structure and peaks that are masked when using the 532 nm laser. The choice of laser wavelength is, however, dependent on the analyte and substrate, and sometimes lower wavelengths are in fact feasible.

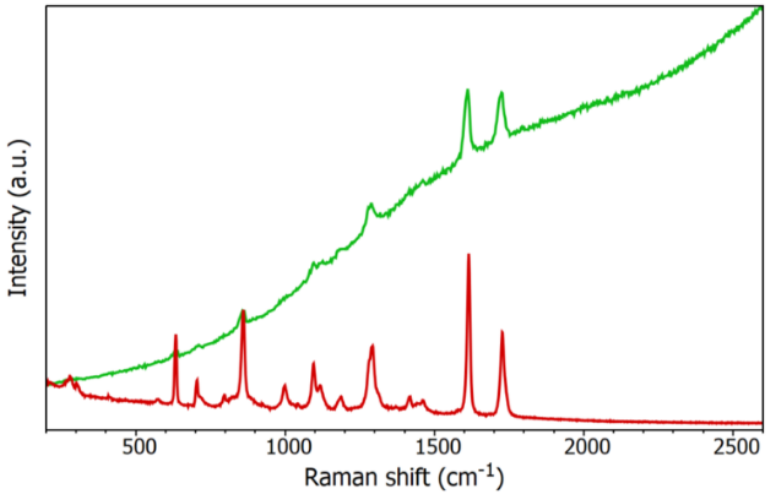

Figure 6: Nicotine patch spectra measured at 532 nm (green) and 785 nm (red). The lower wavelength laser results in high fluorescence interference which almost completely masks the Raman signals. Spectra taken from reference [10].

4 Discussion: Examples of Applications

SERS is very versatile in the sense that it has a wide range of applications in all kinds of fields. A few examples include imaging and microscopy, chemical and biological sensing, forensic science and nanotechnology [17]. Since SERS can detect trace amounts of molecules, it could also be very useful for environmental samples. Three concrete examples of applications within environmental monitoring are briefly discussed below. However, it is important to keep in mind that these are only a very small fraction of this powerful technique's current and potential applications.

4.1 Detection of Micro- and Nanoplastics in Water

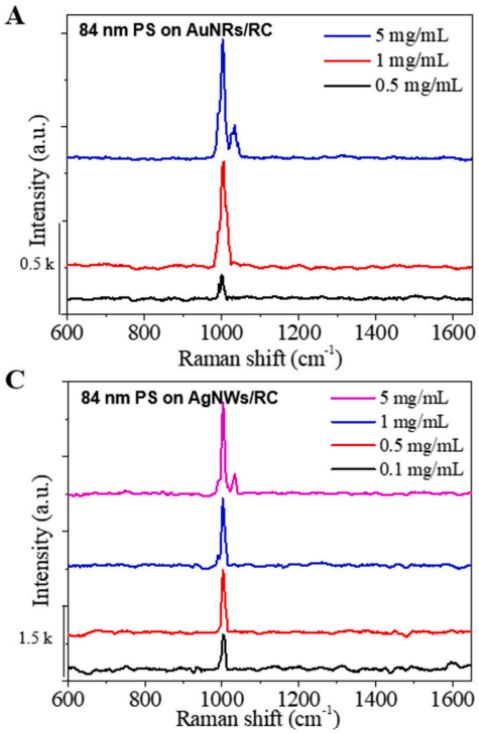

Figure 7: Experimental spectra from the detection of PS nanoparticles with different (known) concentrations on (**A**) AuNRs/RC substrate and (**C**) AgNWs/RC substrate [11]. The latter seems to give a better resolution for this application.

Plastic waste pollution has become a global environmental problem, with significant negative impacts on natural ecosystems and human health. Plastic materials do not biodegrade but break down into smaller particles, called microplastics (MPLs), which are less than 5 mm in size, and nanoplastics (NPLs), which are less than 1 µm in size [26]. These small plastic particles can be found in various environmental compartments, including water, soil, and air, and can be ingested by marine and terrestrial organisms and enter the food chain. Therefore, it is crucial to be able to accurately measure even the smallest concentrations of NPLs in environmental samples to assess the extent of pollution and its potential impacts. The most common forms of plastics found in the sea are polymers of polystyrene (PS), polyethylene (PE), polypropylene (PP) and polyvinyl chloride (PVC) [12].

Conventional analytical techniques, such as Fourier-transform infrared (FTIR) spectroscopy and (standard) Raman spectroscopy are incapable of detecting particles less than about 1 µm in size. Pyrolysis-gas chromatography mass spectrometry is currently a commonly used technique to detect MPLs. However, this technique is destructive and can only analyse small sample sizes. Due to these and other limitations, recent studies have employed SERS as a new method to detect MPLs and NPLs [12]. The SERS substrates used in the detection of NPLs typically consists of two components; metal nanoparticles and high-order metal nanostructure arrays. The latter are arrays of nanostructures arranged in a specific pattern [29].

In one study, Au nanorods (AuNRs) and Ag nanowires (AgNWs) were employed to fabricate regenerated cellulose (RC)-based SERS substrates for the detection of PS nanoparticles [11]. The measurements were performed at a laser wavelength of 785 nm. The Raman spectra obtained for PS particles with a diameter of only 84 nm are shown in figure 7. In this experiment, it was ev-

ident that the AgNWs/RC substrate was superior to the AuNRs/RC substrate as it was able to detect lower concentrations. As can be seen from the figure, the Ag-substrate was able to detect PS-concentrations as low as 0.1 mg/mL PS (equivalent to about 960 nM), while the Au-substrate was incapable of this. The downside to Ag nanoparticles, however, is that the preparation of highly reproducible Ag particles is much more difficult than for Au nanoparticles [29]. For further reading, see reference [11].

4.2 Detection of Polycyclic Aromatic Compounds

Polycyclic aromatic hydrocarbons (PAHs) are a group of organic compounds comprised of two or more fused benzene rings formed by the incomplete combustion of organic materials such as fossil fuels, wood and tobacco. PAHs are ubiquitous and persistent environmental pollutants, and are an increasing concern to human health even at very low concentrations because of their carcinogenicity and mutagenicity [14]. Due to these concerns, it is critical to develop sensitive and cost-effective ways to monitor them. Considering the benefits of SERS discussed, the technique could potentially be used as a reliable approach for monitoring PAHs. However, so far this approach has been somewhat hindered because of the poor adsorption of PAHs onto Ag- and Au-based SERS substrates. Current research is therefore directed towards developing functionalized SERS substrates to improve adsorption [2].

In one study, Ag-based nanoporous substrates with a "coral-like" structure was used to detect pyrene (figure 8) at low concentrations in water [2]. The achieved lower detection limit (LOD) was 23 nM. The measurements were run with a laser wavelength of 532 nm. The three-dimensional (3D) porous substrate provides a large surface area for the exposure of the probe. This gives many hot-spots and possibly extends the concentration range for the analysis to lower values. The substrate was not functionalized to favor the *binding* of the aromatic compounds, but rather to promote the *capture* of them. By capturing the PAHs that adhere to the Ag surface through non-covalent interactions, the first-layer effect could be minimized. The article highlights that the porosity of the substrate is likely the main contributing factor to the experiment's apparent success and suggests that future research on SERS substrates should therefore focus more on the production of porous materials.

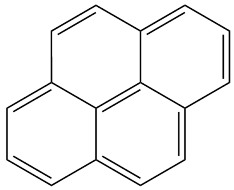

Figure 8: Chemical structure of pyrene, a type of PAH. Drawn in *ChemDraw*.

In another study, four kinds of PAHs were detected on a 3D SERS substrate composed of a porous, hydrophobic polymer material (called GMA-EDMA) with adsorbed gold nanoparticles (57 nm in diameter) [24]. The nanoparticles were added via a syringe as a colloid solution together with different PAH solutions, and the mixture was adjusted to a pH of 13 with sodium hydroxide (NaOH). Low relative standard deviations were obtained from eight substrates, indicating a good repeatability. A SEM image of the substrate is shown in figure 9a. The samples were all measured at a laser wavelength of 785 nm. Obtained SERS and Raman spectra of pyrene are given in 9b. In order to properly evaluate the technique's sensitivity, fluorescence spectroscopy measurements were run on the PAHs. All four PAHs were found to have strong fluorescence. With this information, the minimum detectable concentrations with this SERS method were evaluated to be in the 0.1-1.0 nM range. This high sensitivity, good repeatability and relatively economic and convenient production of the SERS substrate makes the authors conclude that the method has great potential for, amongst others, routine monitoring of environmental pollutants.

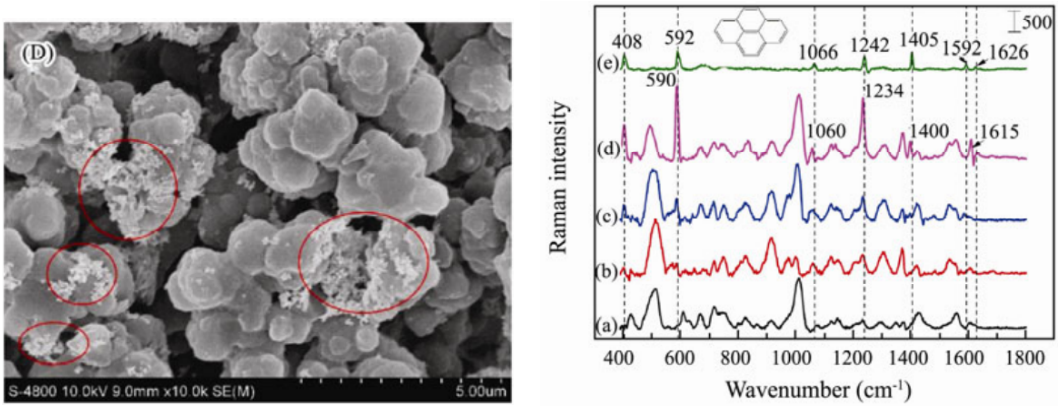

(a) SEM image of GMA-EDMA material with adsorbed Au nanoparticles at pH=13. The pores (black) are about 1 micron in diameter, and the red circles mark huge nanoparticle aggregations.

(b) SERS and Raman spectra of pyrene; (*a*) Raman spectrum of blank probe (only substrate); SERS spectra at concentrations (*b*) 0.3 nM, (*c*) 1 nM, (*d*) 10 nM; (*e*) Raman spectrum of solid pyrene.

Figure 9: SEM image of substrate (left panel) and the SERS spectra of pyrene (right panel) obtained from it. Both images are taken from article [24].

4.3 Detection of Organochlorine Pesticides

Pesticides are chemical compounds used to control pests such as insects, fungi and weeds. These chemicals are typically applied to crops to protect them from damage, but their use is not without risks. Pesticides and their residues can be carried by water and wind and contaminate the environment. Further remedial actions for these residues are necessary to ensure the health of ecosystems and ultimately humans [28]. Organochlorine pesticides (OCPs) were extensively used from the 1940s through the 1960s. They are being phased out globally, but due to their persistent nature, they can still pollute the environment for several years or decades after usage. With the increasing demand of pesticide analysis, SERS has emerged as a powerful candidate for in-field sensitive analysis. Several different strategies for OCP detection using SERS have been developed, with active research focusing on the development of new substrates here as well [19].

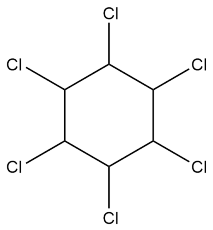

Figure 10: Chemical structure of lindane, a typical OCP. Drawn in *ChemDraw*.

A reusable nanoporous silver (NPAg) sheet is an example of a SERS substrate that has been developed specifically for the detection of OCPs. In one experiment, lindane (figure 10) was chosen as the analyte to test the sheet's performance [3]. The experimental LOD was determined to be 300 nM with an EF in the 10^9-range. All probes were measured with a commercially available 632.8 nm He-Ne laser. The article reflects over several benefits with the NPAg sheet. Firstly, the characteristic region of OCPs are at about 300-400 cm^{-1}, a region where there was no background peak from the sheet itself and thereby decreasing noise interference. Secondly, its porosity gives many potential hot spots. Another important aspect is the substrate's potential reusability when performing specific cleaning treatments. Reusability has gradually become a more and more important

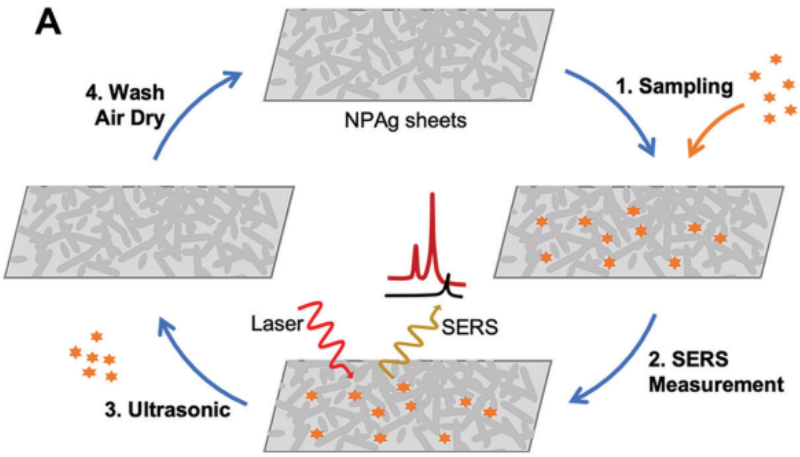

Figure 11: Illustration of a reuse cycle for the NPAg sheet. Figure taken from article [3].

evaluation criterion in the development of low-cost detection methods. It also makes the substrate more environmentally-friendly in comparison to disposable substrates. A typical reuse cycle for the NPAg sheet is shown in figure 11. After applying the sample and performing a SERS measurement, the sheet can be ultrasonically cleaned and air-dried and then reused for another analysis. In the experiment's preliminary tests, the NPAg sheet could be reused for up to 22 cycles. Many more SERS substrates have been developed specifically for the detection of OCPs. For an overview of these, the reader is referred to article [19].

5 Conclusion and Future Perspectives on SERS

The Drude-Lorentz model has been explored to describe the dielectric function of a nanosphere of linear dielectric material, specifically for the case of gold and silver. This was done as an attempt to explain the large enhancement factor in SERS, a phenomenon that to this date is not well-understood. Some technical challenges associated with SERS were also discussed.

SERS has shown great promise as a sensitive and selective analytical technique for environmental monitoring. However, there are several challenges that need to be addressed before the technique can be widely adopted in this and other fields. One of the main challenges is the potential interference of background fluorescence. Various strategies have been developed to overcome this challenge, with the perhaps easiest measure being to use a higher wavelength laser than what theory states to be the optimum. Another challenge in the application of SERS is the need for robust and reproducible SERS substrates. The performance of SERS substrates can vary depending on the fabrication method, substrate morphology, and surface chemistry, which can affect the reproducibility and reliability of SERS measurements. Therefore, active research is being done to develop more reliable, cost-efficient, and environmentally-friendly substrates.

Despite these challenges, the future perspectives of SERS, specifically in environmental monitoring, are promising. SERS has shown great potential for the detection of a wide range of environmental contaminants with both high sensitivity and selectivity. In addition, the development of portable and miniaturized SERS systems has enabled in-situ and real-time monitoring of environmental pollutants, which can provide more comprehensive and accurate data for risk assessment and management. With further advancements in SERS substrate fabrication, instrument design, and data analysis, SERS can be expected to play an increasingly important role in the environmental sciences and monitoring in the future.

References

[1] Hans Bouwmeester, Peter CH Hollman, and Ruud JB Peters. Potential health impact of environmentally released micro-and nanoplastics in the human food production chain: experiences from nanotoxicology. *Environmental science & technology*, 49(15):8932–8947, 2015.

[2] Angela Capaccio, Antonio Sasso, and Giulia Rusciano. Feasibility of sers-active porous ag substrates for the effective detection of pyrene in water. *Sensors*, 22(7):2764, 2022.

[3] Huanyu Chi, Congcheng Wang, Zhien Wang, Hongni Zhu, Vince St Dollente Mesias, Xin Dai, Qing Chen, Wei Liu, and Jinqing Huang. Highly reusable nanoporous silver sheet for sensitive sers detection of pesticides. *Analyst*, 145(15):5158–5165, 2020.

[4] Dr. Colton. Lorentz oscillator model of the dielectric function, 2020. Physics 581, Last updated: Fall 2020.

[5] Claire Deeb. *Optical Properties of Metal Nanostructures as Probed by Photosensitive Molecules*. PhD thesis, 10 2010.

[6] P. Drude. Zur Elektronentheorie der Metalle (German). *Annalen der Physik*, 306(3):566–613, 1900.

[7] David J Griffiths. Introduction to electrodynamics, 2005.

[8] Christian Heck. *Gold and silver nanolenses self-assembled by DNA origami*. PhD thesis, Universität Potsdam, 2017.

[9] Sebastian Heeg, Niclas S Mueller, Sören Wasserroth, Patryk Kusch, and Stephanie Reich. Experimental tests of surface-enhanced raman scattering: Moving beyond the electromagnetic enhancement theory. *Journal of Raman Spectroscopy*, 52(2):310–322, 2021.

[10] Edinburgh Instruments. Lasers for raman spectroscopy. https://www.edinst.com/blog/lasers-for-raman-spectroscopy/, June 2021. Accessed: March 12, 2023.

[11] Youngho Jeon, Dabum Kim, Goomin Kwon, Kangyun Lee, Chang-Sik Oh, Ung-Jin Kim, and Jungmok You. Detection of nanoplastics based on surface-enhanced raman scattering with silver nanowire arrays on regenerated cellulose films. *Carbohydrate Polymers*, 272:118470, 2021.

[12] Nenad Joksimovic, Dragica Selakovic, Nemanja Jovicic, Nenad Jankovic, Periyakaruppan Pradeepkumar, Aziz Eftekhari, Gvozden Rosic, et al. Nanoplastics as an invisible threat to humans and the environment. *Journal of Nanomaterials*, 2022, 2022.

[13] K Lance Kelly, Eduardo Coronado, Lin Lin Zhao, and George C Schatz. The optical properties of metal nanoparticles: the influence of size, shape, and dielectric environment, 2003.

[14] Ki-Hyun Kim, Shamin Ara Jahan, Ehsanul Kabir, and Richard JC Brown. A review of airborne polycyclic aromatic hydrocarbons (pahs) and their human health effects. *Environment international*, 60:71–80, 2013.

[15] Katrin Kneipp. Surface-enhanced raman scattering. *Physics Today*, 60(11):40–46, 2007.

[16] Katrin Kneipp, Harald Kneipp, Irving Itzkan, Ramachandra R. Dasari, and Michael S. Feld. Surface-enhanced raman spectroscopy (sers): Principles, nanostructures, fabrications and biomedical applications. *Journal of Raman Spectroscopy*, 39(3):249–271, 03 2008.

[17] Katrin Kneipp, Martin Moskovits, and Harald Kneipp. *Surface-enhanced Raman scattering: physics and applications*, volume 103. Springer Science & Business Media, 2006.

[18] Eric Le Ru and Pablo Etchegoin. *Principles of Surface-Enhanced Raman Spectroscopy: and related plasmonic effects*. Elsevier, 2008.

[19] Rebeca Moldovan, Bogdan-Cezar Iacob, Cosmin Farcău, Ede Bodoki, and Radu Oprean. Strategies for sers detection of organochlorine pesticides. *Nanomaterials*, 11(2):304, 2021.

[20] David Morin. *Introduction to classical mechanics: with problems and solutions*. Cambridge University Press, 2008.

[21] Lutz Nasdala, David C Smith, Reinhard Kaindl, Martin A Ziemann, A Beran, E Libowitzky, et al. Raman spectroscopy: analytical perspectives in mineralogical research. *Spectroscopic methods in mineralogy*, 6:281–343, 2004.

[22] Ron Schmitt. *Electromagnetics explained: a handbook for wireless/RF, EMC, and high-speed electronics*. Newnes, 2002.

[23] Bhavya Sharma, Renee R Frontiera, Anne-Isabelle Henry, Emilie Ringe, and Richard P Van Duyne. Sers: Materials, applications, and the future. *Materials Today*, 15(1-2):16–25, 2012. Open access under CC BY-NC-ND license.

[24] Xiaofeng Shi, Xia Yan, Xinmin Zhang, Lizhen Ma, Xu Zhang, Chunyan Wang, and Jun Ma. Ultrasensitive detection of polycyclic aromatic hydrocarbons (pahs) in water using three-dimensional sers substrate based on porous material and ph 13 gold nanoparticles. *Journal of Ocean University of China*, 18:1523–1531, 2019.

[25] Paul L Stiles, Jon A Dieringer, Nilam C Shah, and Richard P Van Duyne. Surface-enhanced raman spectroscopy. *Annu. Rev. Anal. Chem.*, 1:601–626, 2008.

[26] Lynn R. Terry, Sage Sanders, Rebecca H. Potoff, Jacob W. Kruel, Manan Jain, and Huiyuan Guo. Applications of surface-enhanced raman spectroscopy in environmental detection. *Analytical Science Advances*, 3(3-4):113–145, 2022.

[27] Kaidi Wang, Shenmiao Li, Marlen Petersen, Shuo Wang, and Xiaonan Lu. Detection and characterization of antibiotic-resistant bacteria using surface-enhanced raman spectroscopy. *Nanomaterials*, 8(10):762, 2018.

[28] Ting Wang, Shuangpeng Wang, Zehua Cheng, Jinchao Wei, Lele Yang, Zhangfeng Zhong, Hao Hu, Yitao Wang, Bingpu Zhou, and Peng Li. Emerging core–shell nanostructures for surface-enhanced raman scattering (sers) detection of pesticide residues. *Chemical Engineering Journal*, 424:130323, 2021.

[29] Lifang Xie, Kedong Gong, Yangyang Liu, and Liwu Zhang. Strategies and challenges of identifying nanoplastics in environment by surface-enhanced raman spectroscopy. *Environmental Science & Technology*, 2022.

[30] Bedir B Yousif and Ahmed S Samra. Optical responses of plasmonic gold nanoantennas through numerical simulation. *Journal of nanoparticle research*, 15:1–15, 2013.

[31] Clement Yuen, Wei Zheng, and Zhiwei Huang. Surface-enhanced raman scattering: Principles, nanostructures, fabrications, and biomedical applications. *Journal of Innovative Optical Health Sciences*, 1(02):267–284, 2008.